
A computational study of vortex shedding from a NACA-0012 airfoil at high angles of attack

Mohamed Y. Zakaria*

Aerospace Engineering Department,
Military Technical College,
11766, Cairo, Egypt
Email: zakaria@mtc.edu.eg
*Corresponding author

Mostafa M. Ibrahim

Mechanical Power Engineering Department,
Faculty of Engineering,
Zagazig University,
Zagazig, Egypt
Email: dr.moustafa48@gmail.com

Saad Ragab and Muhammad R. Hajj

Engineering Mechanics Program,
Virginia Tech.,
Blacksburg, 24061, USA
Email: ragab@vt.edu
Email: mhajj@vt.edu

Abstract: A numerical investigation of the two-dimensional flow over a NACA-0012 wing section is conducted at Reynolds number of 79,900 over a range of angles of attack between zero and 40 degrees. The performance of different turbulence models in terms of capturing flow separation and transition, and vortex shedding at 40 degrees is determined. Three turbulence models, namely the Spalart-Allmaras (SA), modified Spalart-Allmaras, and Reynolds stress transport model and a simulation without a turbulence model (laminar flow) are conducted. The results show that the lift and drag coefficients predicted by the Spalart-Allmaras model are in good agreement with experimental data; with small differences over angles of attack larger than 25 degrees. The Reynolds stress transport model and laminar flow calculations predict vortex shedding from the leading and trailing edges and formation of a vortex street in the wake. On the other hand, simulations using the Spalart-Allmaras and modified Spalart-Allmaras models do not predict such a vortex wake and that may be due to over-diffusion of shed vortices. Power spectral densities of the unsteady lift, drag and velocity are used to determine flow characteristics and their relation to the forces.

Keywords: high angle of attack; wind tunnel testing; turbulence models; vortex shedding.

Reference to this paper should be made as follows: Zakaria, M.Y., Ibrahim, M.M., Ragab, S. and Hajj, M.R. (2018) 'A computational study of vortex shedding from a NACA-0012 airfoil at high angles of attack', *Int. J. Aerodynamics*, Vol. 6, No. 1, pp.1–17.

Biographical notes: Mohamed Y. Zakaria is currently an Assistant Professor in Aerospace Department at the Military Technical College. He earned his PhD on May 2016 from the Virginia Tech. His has a wide research interests that cover applied aerodynamics, experimental unsteady aerodynamics, energy harvesting from fluid flow, and wind tunnel testing.

Mostafa M. Ibrahim is currently an Assistant Professor in the Mechanical Power Department, Faculty of Engineering at Zagazig University. He earned his PhD on April 2011 from the Zagazig University. His research area includes aerodynamics, computational fluid dynamics, heat transfer.

Saad Ragab is a Professor in the Department of Biomedical Engineering and Mechanics, Virginia Tech. He earned his PhD degree from the Virginia Tech in 1979. His research area includes aerodynamics, computational fluid dynamics, turbulence simulations, and multiphase flows. Recently, he published a textbook, *Introduction to Finite Element Analysis for Engineers*, co-authored with Dr. Hassan Fayed, and published by CRC, 2017.

Muhammad R. Hajj is a J. Byron Maupin Professor of Engineering at the Virginia Tech. His research is focused fluid flows and fluid structure interactions with applications to bio-inspired flight and locomotion and to harvesting fluidic power.

1 Introduction

Airfoil aerodynamics in the stall and post-stall regimes exhibit complex aspects that are strongly dependent on the Reynolds number and angle of attack. This is especially true in the low Reynolds number regime between 10^4 and 3×10^5 where the flow exhibits separation, transition to turbulence of the separated shear layer and potentially vortex shedding depending on the angle of attack. These aspects are of utmost importance when optimising the performance of blades of propellers and wind turbines or wings of micro and unmanned air vehicles. The complexities are further pronounced when considering dynamic variations in the angle of attack as in the case of insect and bird flight, flapping micro-air vehicles (Ghommem et al., 2012; Zakaria et al., 2014; Taha et al., 2014), in determining flight boundaries and for the purpose of energy harvesting (Zakaria et al., 2015a), lift enhancement (Zakaria et al., 2015b, 2016, 2017) or prediction of dynamic stall (Mittal and Saxena, 2000). Noteworthy also is the fact that these variations are further amplified when considering operational conditions such as high turbulence intensities (Lee and Markus, 1976; Wang et al., 2004). Vortex shedding from airfoils in the low Reynolds number regime has been noted in several experimental studies. Huang and Lin (1995) observed vortex shedding in the flow over a NACA-0012 airfoil at angles of attack beyond 15 degrees. Using the classifications of Huang and Lin (1995) and Lee

and Huang (1998) of laminar, subcritical, transitional and supercritical vortex shedding, Rodríguez et al. (2013) concluded that the flow over a NACA-0012 at $Re = 5 \times 10^4$ is characterised by incoherent vortex shedding (transitional mode) when the angle of attack is 9.25 degrees and more coherent vortex shedding (supercritical mode) at 12 degrees. Coherent structures and vortex shedding were also observed in this range of Reynolds number in the flow over a NACA-0018 airfoil at angles of attack below 10 degrees by Yarusevych and Boutilier (2011) and over a NACA-0025 airfoil at an angle of attack of 10 degrees by Yarusevych et al. (2009).

Experimental measurements and numerical simulations of the lift and drag forces and wake characteristics of the flow over airfoils in the low Reynolds number regime at stall and post stall angles of attack have not been as extensive as flows at low angles of attack. Lee and Huang (1998) determined that the variation of the Strouhal number with the Reynolds number is different at high angles of attack than at low angles of attack. Zhou et al. (2011) presented data of mean and fluctuating forces on a NACA-0012 airfoil over a broad range of angles of attack up to 90 degrees at $Re = 5,000$ and $50,000$. Alam et al. (2010) performed experiments on the flow structure in the wake of a NACA-0012 airfoil under the same operating conditions as Zhou et al. (2011). They presented force and wake measurements and discussed the vortex formation and shedding and variations in its frequency and size with the angle of attack.

Numerical simulation of flows that exhibit complex characteristics such as separation, transition of the separated shear layer and vortex shedding can be performed with different levels of fidelity. High-fidelity simulations such as large eddy simulation (LES) (El-Okda et al., 2008; Ayed et al., 2015) and direct numerical simulation (DNS) require fine grids and are computationally expensive. A more common approach is to use the Reynolds-averaged navier-stokes (RANS) with different models for the Reynolds stresses. In one-equation models such as the Spalart-Allmaras (SA) model (Spalart and Allmaras, 1992), the Reynolds shear stress tensor is modelled in terms of the mean strain and eddy viscosity. In two-equation models, the eddy viscosity is modelled in terms of the kinetic energy and another variable such as dissipation, which results in two equations for the kinetic energy and dissipation that are then solved simultaneously. Because the performance of these models can be application-dependent, there has been recent interest in evaluating their use and their ability to predict turbulent separated flows, evolution of free shear flows and shock-boundary layer interactions (Slotnick et al., 2014). Dudek and Carlson (2017) compared simulation results based on one-equation SA model and two-equation menter shear stress transport model of different flows with experimental results and found that the level of their performance is application dependent. Using Reynolds averaged navier stokes equations, Wells et al. (2009) highlighted the effects of turbulence modelling on the simulations of vortical wake flows such as the rolled-up vortices in the near wake of a rectangular wing. They concluded that, simulations with the full Reynolds stress model (RSM) yield a remarkable mean flow agreement with experimental data in the tip vortex and spiral wake due to the proper prediction of a laminar vortex core. Simulations with the SA model predicted over-diffusion of the tip-vortex. This was explained by their evaluation that the SA model should be corrected to deal with the eddy viscosity term for rotating flows.

In present effort, we evaluate the performance of the SA and full RSMs in predicting the flow over a NACA-0012 airfoil in the low-Reynolds number regime. Particularly, we compare the experimental static lift and drag results presented by Zakaria et al. (2015b) with results obtained from SA model at the same Reynolds number. Then, we compare the performance of four different models, namely the laminar flow, SA, modified SA and Reynolds stress transport models, in the analysis of the flow structure of the 2D wake over a NACA-0012 airfoil at 40° angle of attack and $Re = 79,900$. This comparison is important because using an inappropriate model might lead to failure in capturing the associated shedding frequencies at high angles of attack. The evaluation of each of the four simulations is based on the prediction of mean flow quantities such as lift and drag and complex flow and wake structure associated with this flow.

2 Experiments

The experiments were conducted in an open-jet-return, low speed wind tunnel. The test chamber has a cross section of $0.7\text{ m} \times 0.7\text{ m}$ and a length of 1.5 m . The tunnel free stream turbulence intensity is 1% at the operating speed $U_\infty = 8.6\text{ m/s}$, which corresponds to a chord Reynolds number of $79,900$. The flow speed is controlled by an AF600 General Electric variable frequency drive. The designed mechanism was controlled to allow for varying the mean angle of attack, α_0 , between 0° and 65° . A foam core NACA 0012 was machined using a laser cutter and reinforced with a carbon fibre rod of diameter 4 mm at quarter chord location and the whole profile was covered by two layers of carbon fibre fabric. The wing has an aspect ratio of 4.5 with a chord length of 0.14 m and a span of 0.63 m . The wing model was mounted horizontally in the centre of the test section. We used end plates (each plate is 0.25 m long and 0.15 m wide) to ensure two-dimensional flow within 2.7%. Wind tunnel blockage was less than 3.7% when the airfoil was set at the maximum angle of attack.

Figure 1 Experimental setup of naca-0012 in the wind tunnel facility (see online version for colours)



Source: Zakaria et al. (2017)

The wind tunnel is equipped with a six component strain gauge balance of strut model support system having an accuracy of 1.2% (0.05 N). The data were collected and processed using a sampling frequency rate of 2,500 Hz. The measured signals were amplified by a transducer amplifier and connected to a National Instruments SCXI 1520 Multifunction DAQ. Force measurements were ensemble averaged over three experiments and force coefficients were evaluated in terms of the dynamic pressure corresponding to the steady-state velocity, U_∞ . A digital protractor was used to measure the wing's setting angle with an error of $\pm 0.2^\circ$.

Figure 2 Comparison of the current steady C_L -measurements with theory and other experimental results (see online version for colours)

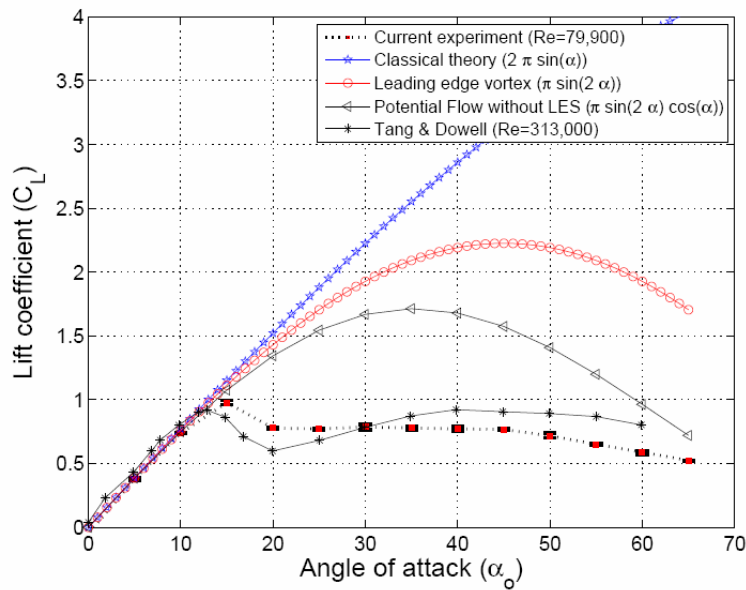


Figure 2 shows a comparison of the current measurements of the static lift curve at $Re = 79,900$ with the measurements of Tang and Dowell (2014) at $Re = 313,000$, and theoretical predictions. These predictions include those of the classical airfoil theory $C_L = 2\pi \sin \alpha$, the potential flow lift without leading edge suction $C_L = 2\pi \sin \alpha \cos^2 \alpha$ (Polhamus, 1966), and the fit of the static lift due to a stabilised leading edge vortex $C_L = 2\pi \sin 2\alpha$, proposed by Berman and Wang (2007). Based on standard statistical evaluation methods (assuming Gaussian distribution of data), uncertainty limits with a 95% confidence level were determined for each of the load measurements based on three separate runs. The plots show that the current experimental measurements are in a qualitative agreement with the measurements of Tang and Dowell (2014). Both measurements match predictions of the classical wing theory over its range of applicability up to ten. The slight difference in the maximum lift between the current measurements and that of Tang and Dowell (2014) can be attributed to the difference in the Reynolds numbers. For a purely two-dimensional flow, a stabilised leading edge vortex that augments the lift cannot be realised under static conditions. As such, the predictions of the lift due to a stabilised leading edge vortex, given by $C_L = 2\pi \sin 2\alpha$, are

higher than the current measurements. Finally, the potential flow model without leading edge suction overestimates the generated lift as it does not account for the separation effects.

3 RANS simulations

3.1 Turbulence models

The SA model is a relatively simple one-equation model that solves a modelled transport equation for the kinematic eddy (turbulent) viscosity. Dacles-Mariani et al. (1995) and (1999) modified the SA model to account for the numerical error associated with the vortex shedding. The modified model is a vorticity-strain based model (*rotation correction*). The modification should be passive in thin shear layers where vorticity and strain are very close. The RSM is a more elaborate turbulence model. Abandoning the isotropic eddy viscosity hypothesis, the RSM closes the Reynolds-averaged Navier-Stokes equations by solving transport equations for the Reynolds stresses, together with an equation for the dissipation rate. This means that five additional transport equations are required in two-dimensional flows and seven additional transport equations must be solved in three dimensional flows. Because the RSM accounts for the effects of streamline curvature, swirl, rotation, and rapid changes in strain rate in a more rigorous manner than one-equation and two-equation models, it has a greater potential to give accurate predictions for complex flows (Taulbee, 1992). The use of the RSM is a must when the flow features of interest are the result of anisotropy in the Reynolds stresses. Among the examples are cyclone flows, highly swirling flows in combustors, rotating flow passages, and the stress-induced secondary flows in ducts.

3.2 Computational domain and mesh sensitivity

ANSYS Fluent 15 is used to simulate the flow over a NACA-0012 airfoil over a broad range of angles of attack between zero and 40° . As shown in Figure 3, the solution was performed over a domain that extended over an area of at least 12.5 chord lengths around the airfoil. The domain Dirichlet conditions were used at the inlet boundary and a pressure outlet condition was used at the outlet boundary. The mesh was generated using the GAMBIT modeller. Figure 4 illustrates the global mesh boundaries around the airfoil and a zoomed view for the shedding line inclined at 40° from the airfoil chord with a length of five chords. As shown in the figure, a higher grid resolution is used near the airfoil surface and in its wake to resolve the boundary layer and capture the wake characteristics to yield an acceptable computational accuracy. To determine a satisfactory number of mesh nodes, we performed simulations whereby the number of nodes was increased until further refinement of the mesh produced negligible changes. Tables 1 and 2 show variations of the values of the mean lift and drag coefficients as the number of nodes was increased respectively for angles of attack of 5° and 40° . The numbers show that a grid of 520,000 nodes is sufficient to yield converging values for these coefficients. This resolution is also acceptable for a shedding line of 40° as it covers at least five chords along this line. Although the finest region of the grid is not aligned with this shedding direction, the grid is still fine enough to resolve shed vortices at this high angle of attack.

Figure 3 Computational domain for NACA-0012 (see online version for colours)

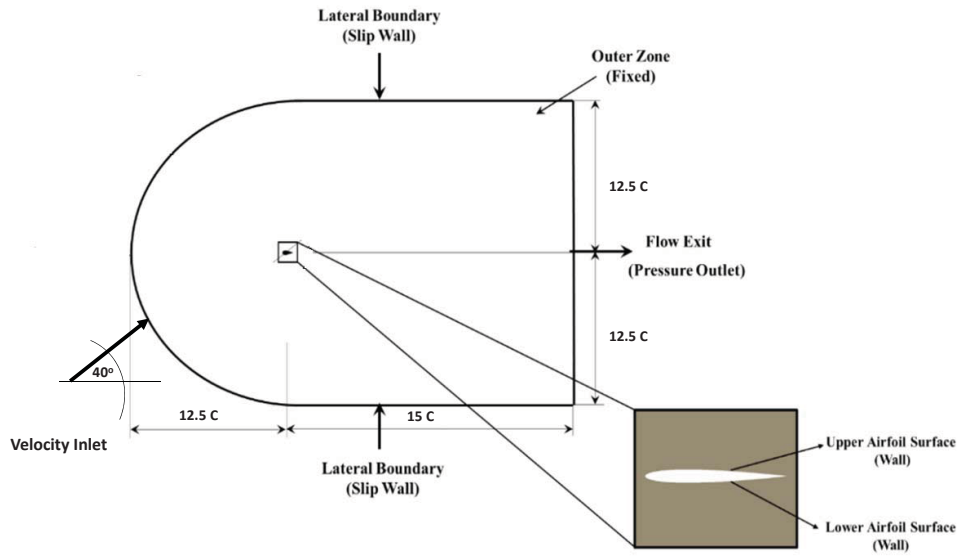
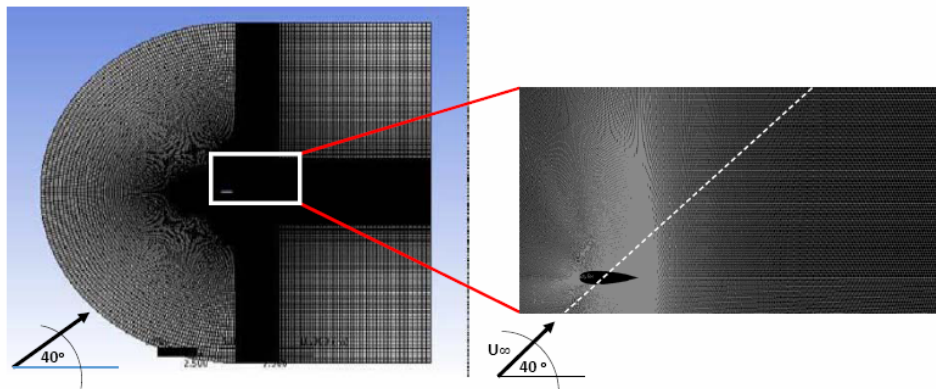


Figure 4 Grid generation using gambit software, 520,000 elements (see online version for colours)



3.3 Force coefficients

Variations in the mean lift and drag coefficients with the angle of attack up to 40° obtained from the SA model are compared with the experimental measurements in Figure 5. The results show good agreement with the wind tunnel data and captures the same trend at stall conditions. Each simulation point corresponds to an average value over the simulation time record excluding the transient time steps. We note that the simulated values of the lift coefficient are slightly higher in the range between 25° to 40° . As will be shown below, the SA model fails to simulate the vortex shedding at these high angles of attack. Table 3 shows a comparison of experimental values of the lift and drag coefficients with predicted values from three selected simulations (SA, laminar and

RSM). Based on the calculated percentage differences, we conclude that all simulations predict acceptable mean values with the SA model yielding the largest departure from the measured value of 5.5% in the lift coefficient.

Table 1 Sensitivity analysis of the variation of the simulated mean values of the lift and drag with the number of nodes in the mesh

Mesh elements (10^3)	C_L	C_D
62	0.492	0.042
129	0.489	0.033
256	0.475	0.032
332	0.478	0.031
520	0.480	0.031

Note: The simulations were carried out using the SA computational model. The angle of attack is 5° and $Re = 79,000$.

Table 2 Sensitivity analysis of the variation of the simulated mean values of the lift and drag with the number of nodes in the mesh

Mesh elements (10^3)	C_L	C_D
62	1.0917	0.8759
129	1.0211	0.8454
256	0.983	0.8315
332	0.925	0.8241
520	0.873	0.8190
560	0.868	0.8115

Note: The simulations were carried out using the SA computational model. The angle of attack is 40° and $Re = 79,000$.

Figure 5 Static mean lift and drag coefficients compared with CFD simulation using SA model at $Re = 79,900$ for NACA-0012, (a) static lift curve (b) static drag curve (see online version for colours)

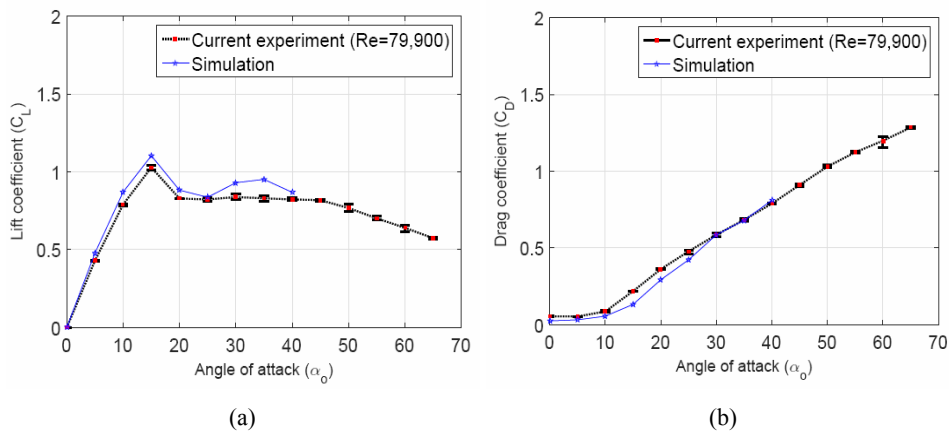
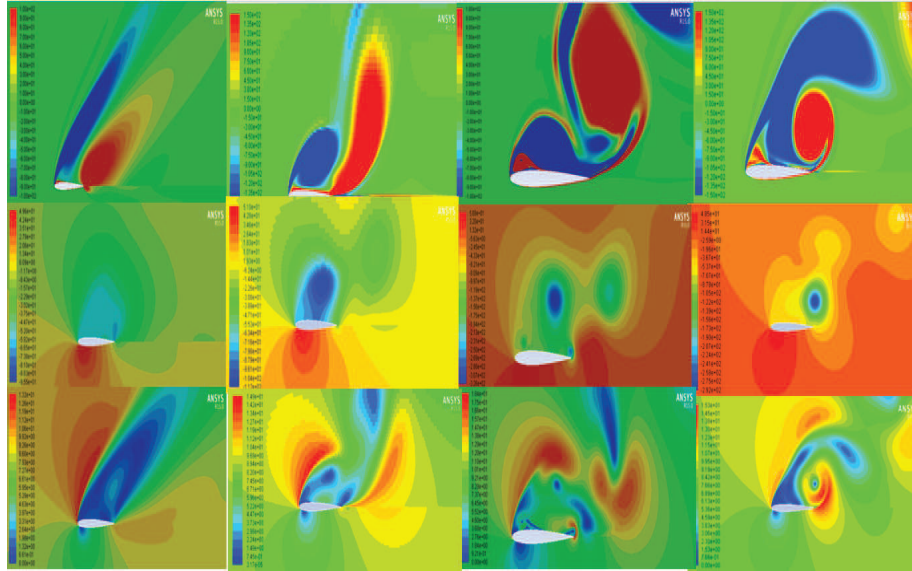


Figure 6 Models comparison for NACA 0012 at $Re = 79,900$ and $\alpha_o = 40^\circ$ (SA, SA modified, laminar, Reynolds stress) (see online version for colours)



Note: First row (vorticity contours), second row (pressure contours) and third row (velocity contours).

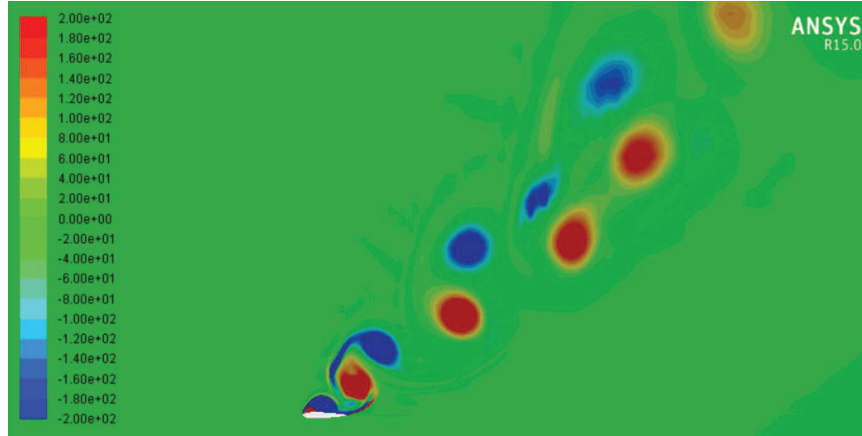
Table 3 Comparison of force coefficients predicted with three selected models (SA, Laminar and RSM) and experimentally measured values at $AoA = 40^\circ$ and $Re = 79,000$

Model	C_L	C_D	$diff(C_L)$ (%)	$diff(C_D)$ (%)
Experiments	0.822	0.7892	–	–
SA	0.868	0.8115	5.5	2.7
Laminar	0.8	0.84	2.6	6.4
RSM	0.79	0.81	3.8	2.66

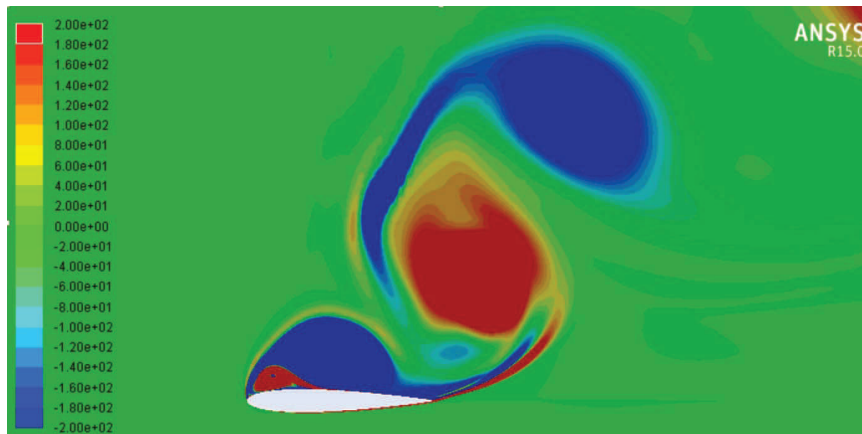
3.4 Flow field characteristics

Next, we compare the flow field characteristics at a high angle of attack using four different simulations (SA, SA modified, laminar and RSM) to determine their ability to capture the vortex shedding in the wake. The first, second and third rows of Figure 6 show respectively the vorticity, pressure and velocity contours. The first, second, third and fourth columns of the same figure show the predicted contours with the SA, SA modified, laminar flow and Reynold Stress Model, respectively. It is clear from all contours that the SA and SA modified models fail to simulate the vortex shedding as obtained from the laminar flow and RSM simulations. This is most likely due to the over-diffusion of the shed vortices as noted by Wells et al. (2009). These two latter simulations have almost the same flow structures. Zoomed views of the flow domain presented in Figures 7 and 8 clearly show the vortex shedding as simulated respectively by laminar flow and RSM.

Figure 7 Vorticity contours for laminar flow at $Re = 79,900$ for NACA-0012 at $\alpha_o = 40^\circ$, (a) vorticity contours zoomed out view (b) vorticity contours zoomed in view (see online version for colours)



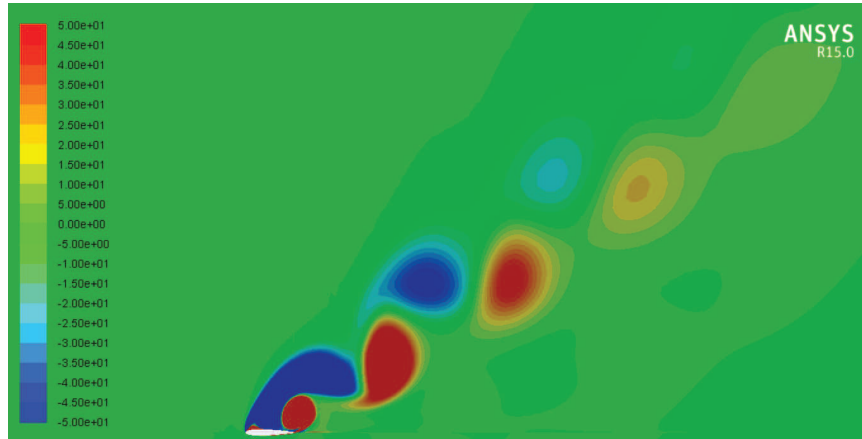
(a)



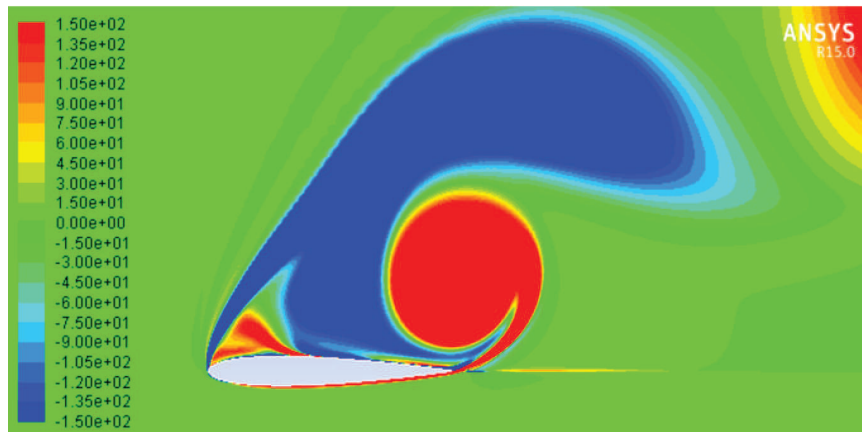
(b)

Figures 9 and 10 show time series of the lift and drag coefficients for both laminar flow and RSM simulations over a period of 0.9 seconds. Figure 11 shows the power spectral density (PSD) corresponding to the time series shown in Figures 9 and 10. Both laminar flow and RSM simulations yield the same shedding frequency, f_s , of about 14 Hz, which is equivalent to a Strouhal number of 0.22. This predicted value is close to the measured value of 0.232 reported by Alam et al. (2010) for a flow over a NACA-0012 airfoil at an angle of attack of 40° and $Re = 10,500$. The force coefficient spectra also show a well-defined peak at twice the shedding frequency, $2f_s$. Spectra of the velocity at specific locations in the wake shown below will also show peaks at f_s and $2f_s$. The second harmonic ($2f_s$) is shown to be due to the secondary vortices induced on the upper surface by the primary vortices shed from the leading and trailing edges.

Figure 8 Vorticity contours using RS model at $Re = 79,900$ for NACA-0012 at $\alpha_o = 40^\circ$, (a) vorticity contours zoomed out view (b) vorticity contours zoomed in view (see online version for colours)



(a)



(b)

In order to characterise the vortex shedding in the wake, we collected time history fluctuations for the X-velocity component at different locations in the vicinity of the airfoil and in its wake as shown in Figure 12. These locations were chosen to capture flow physics along the shear layer separating from the leading edge, near the trailing edge and along a line where vortex shedding takes place as noted when superposing the locations on the flow field as shown in Figure 13. The figure shows six sequential vorticity contours obtained from the RSM simulations with a time step of 0.01 seconds at 40° angle of attack. At the first time step, the free shear layer emanating from the leading edge rolls up into a large vortex on the suction side. At the same time, the boundary layer on the pressure side also separates and rolls around the sharp trailing edge forming a trailing edge vortex. As the later vortex forms it nips the suction side vortex and

subsequently breaks off from the suction side. The two vortices (the trailing edge and the nipped part of the suction side vortex) shed into the wake as a pair of counter rotating vortices. Once the two vortices are shed, the suction side vortex matures again by the vorticity of the feeding separated shear layer from the leading edge. The cycle of trailing edge vortex nipping the suction side vortex and the pair of vortices shedding into the wake repeats. The close proximity of primary vortices (from LE to TE) to the upper surface induces secondary vortices of opposite sign.

Figure 9 Force coefficients using laminar model at $Re = 79,900$ for naca-0012 at $\alpha_o = 40^\circ$, (a) lift coefficient time history using laminar transient model (b) drag coefficient time history using laminar transient model (see online version for colours)

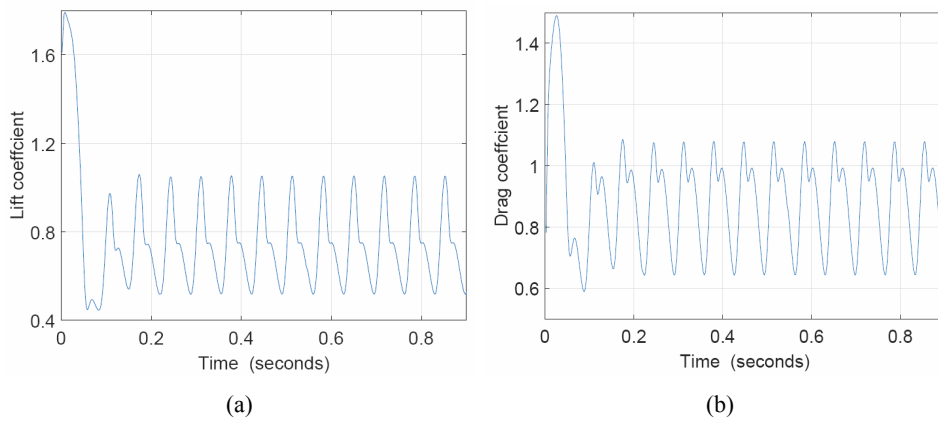
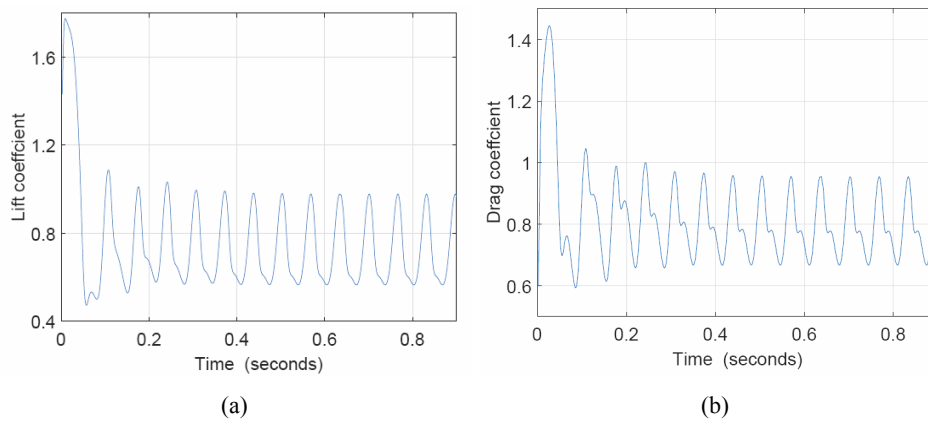


Figure 10 Force coefficients using RS model at $Re = 79,900$ for NACA-0012 at $\alpha_o = 40^\circ$, (a) lift coefficient time history using RS model (b) drag coefficient time history using RS model (see online version for colours)



Figures 14 and 15 show the power spectra for the X component velocity at the selected probe positions shown in Figure 12. Figures 14(a) and 15(a) show the spectra at locations 1 to 6 close to the airfoil surface. Spectra of the velocity components at locations 1, 2, and 3 near the separated shear layer do not exhibit a peak at the shedding frequency. On

the other hand, the velocity spectra at locations 4, 5, and 6 exhibit a clear peak at the shedding frequency.

Figure 11 PSD of lift and drag history for NACA-0012 simulated with laminar model and RSM at 40° angle of attack, (a) power spectra for lift and drag coefficients using laminar transient model (b) power spectra for lift and drag coefficients using RS transient model (see online version for colours)

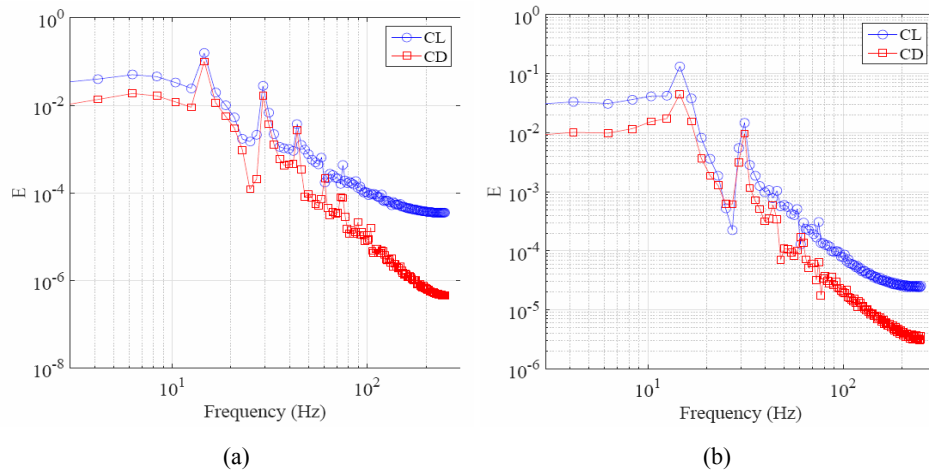
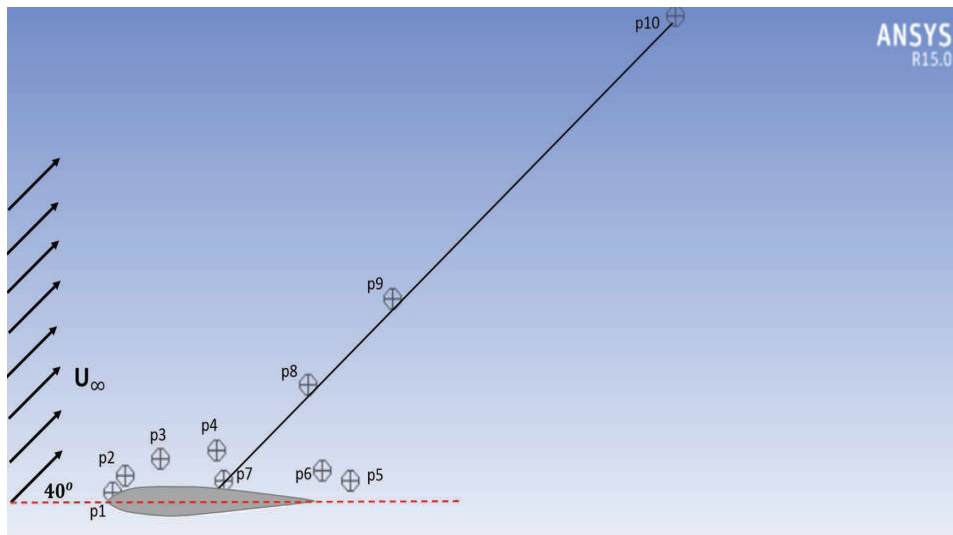


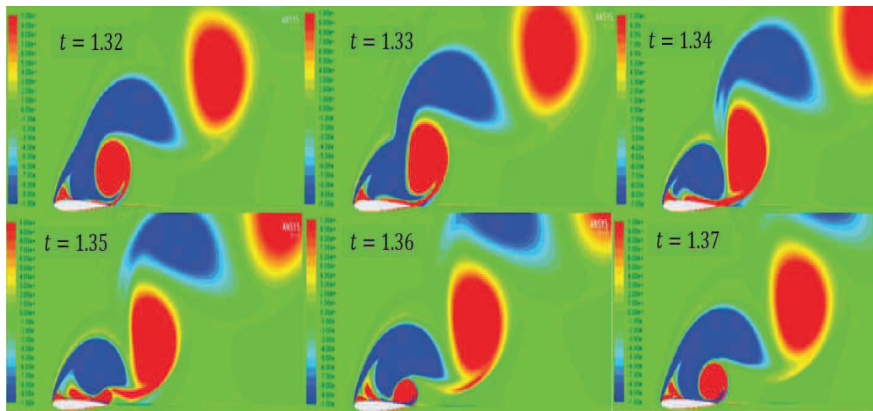
Figure 12 Selected locations for recording the x-velocity component time history fluctuations over NACA-0012 at $Re = 79,900$, $\alpha_o = 40^\circ$ (see online version for colours)



Linear stability analysis of the local velocity profile in the shear layer shows that it is unstable, as expected, but the most amplified frequency is much higher than the shedding frequency. Consequently, at 40-degree angle of attack, the free shear layer separated from the leading edge rolls up into large vortex before it develops the classical

mixing-layer type instabilities. Figures 14(b) and 15(b) show spectra at locations 7 to 10 on the line inclined to the airfoil chord and parallel to the free stream velocity. At these locations, the peak in the spectra is at the same frequency noted at locations 4, 5, and 6. The local peaks at $2f_s$ are due to secondary vortices induced on the upper surface. These results explain the lift enhancement case for an airfoil oscillating in plunge at reduced frequency near 0.7 ($k = 2\pi f_c / U_\infty$) reported by Zakaria et al. (2015b). This could be attributed as a lock-in phenomenon that occurs between the oscillation and shedding frequencies that corresponds to a plunging frequency of \square 14 Hz and was found to be close to the frequency obtained from simulations.

Figure 13 Vorticity time stepping for RS model over NACA-0012 at $Re = 79; 900$, $\alpha_o = 40^\circ$ ($\delta t = 0.01$ s) (see online version for colours)



Note: The locations where velocity time series were collected are superimposed on the plots as black dots and have the same arrangement presented in Figure 12.

Figure 14 PSD of x-velocity component time history for NACA-0012 simulated with RSM at specific locations shown in Figure 12, (a) probes 1 to 6 (b) probes 7 to 10 (see online version for colours)

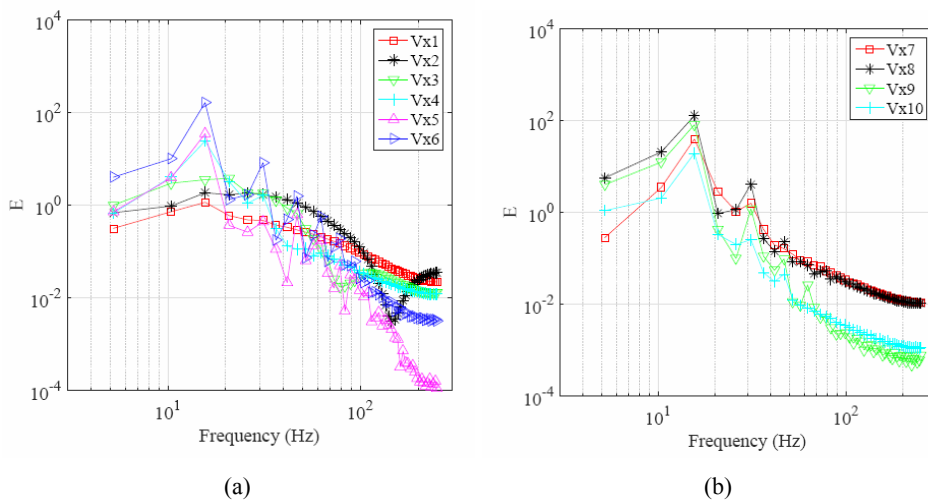
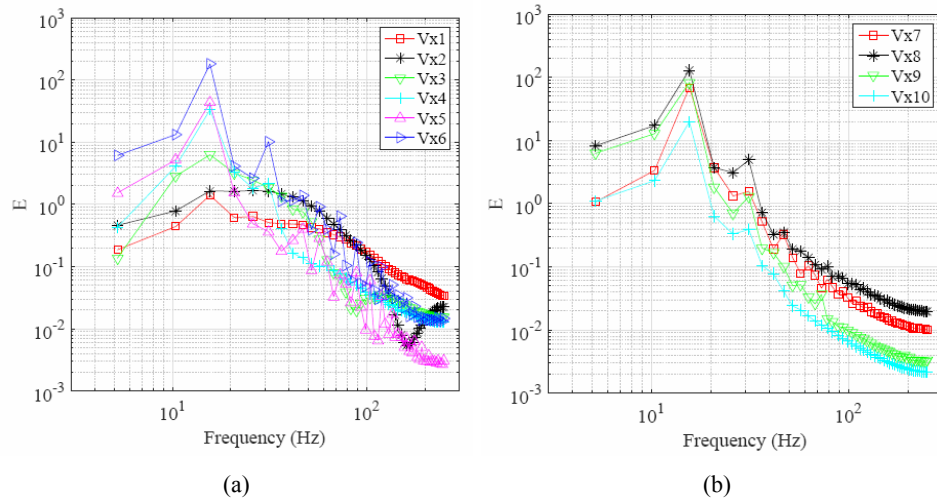


Figure 15 PSD of x-velocity component time history for NACA-0012 simulated with laminar flow model at specific locations shown in Figure 12, (a) probes 1 to 6 (b) probes 7 to 10 (see online version for colours)



4 Conclusions

The performance of different turbulence models in terms of capturing flow separation and transition, and vortex shedding associated with the flow field over NACA-0012 airfoil at a Reynolds number of 79,900 is determined. The turbulence models include the SA model, modified SA model, and the RSM. Additionally, a simulation without a turbulence model is performed. The results showed that all simulations predict averaged lift and drag coefficients that are in agreement with experimental data. Simulations using the SA model yield a lift coefficient that is slightly larger than the measured one at angles of attack between 25° and 40°. Simulations based on the Reynolds stress transport model and laminar flow calculations predict vortex shedding from the leading and trailing edges and the formation of a vortex street in the wake. Simulations with the SA model or its modified form did not predict such a vortex wake indicating over-diffusion of the vorticity. The power spectral densities of the unsteady lift, drag, and velocity reveal that the value of the Strouhal number associated with the vortex shedding frequency is close to a value measured in previous experiments.

References

- Alam, M.M., Zhou, Y., Yang, H., Guo, H. and Mi, J. (2010) ‘The ultra-low Reynolds number airfoil wake’, *Experiments in Fluids*, Vol. 48, No. 1, pp.81–103.
- Ayed, S.B., Ragab, S.A. and Hajj, M.R. (2015) ‘Flow control of extreme pressure loads associated with flow separation’, *Journal of Engineering Mechanics*, Vol. 142, No. 2, p.04015068.
- Berman, G.J. and Wang, Z.J. (2007) ‘Energy-minimizing kinematics in hovering insect flight’, *Journal of Fluid Mechanics*, Vol. 582, No. 1, pp.153–168.

- Dacles-Mariani, J., Kwak, D. and Zilliac, G. (1999) 'On numerical errors and turbulence modeling in tip vortex flow prediction', *International Journal for Numerical Methods in Fluids*, Vol. 30, No. 1, pp.65–82.
- Dacles-Mariani, J., Zilliac, G.G., Chow, J.S. and Bradshaw, P. (1995) 'Numerical/experimental study of a wingtip vortex in the near field', *AIAA Journal*, Vol. 33, No. 9, pp.1561–1568.
- Dudek, J.C. and Carlson, J-R. (2017) 'Evaluation of full Reynolds stress turbulence models in fun3d', in *55th AIAA Aerospace Sciences Meeting*, p.0541.
- El-Okda, Y., Ragab, S. and Hajj, M. (2008) 'Large-eddy simulation of flow over a surface-mounted prism using a high-order finite-difference scheme', *Journal of Wind Engineering and Industrial Aerodynamics*, Vol. 96, No. 6, pp.900–912.
- Ghommem, M., Hajj, M.R., Mook, D.T., Stanford, B.K., Beran, P.S., Snyder, R.D. and Watson, L.T. (2012) 'Global optimization of actively morphing flapping wings', *Journal of Fluids and Structures*, 31 August, Vol. 33, pp.210–228.
- Huang, R.F. and Lin, C.L. (1995) 'Vortex shedding and shear-layer instability of wing at low-Reynolds numbers', *AIAA Journal*, Vol. 33, No. 8, pp.1398–1403.
- Lee, E.B. and Markus, L. (1976) *Foundations of Optimal Control Theory*, Minnesota Minneapolis Center for Control Sciences, December.
- Lee, H-W. and Huang, R-F. (1998) 'Frequency selection of wake flow behind a NACA-0012 wing', *Journal of Marine Science and Technology*, Vol. 6, No. 1, pp.29–37.
- Mittal, S. and Saxena, P. (2000) 'Prediction of hysteresis associated with static stall of an airfoil', *AIAA Journal*, Vol. 38, No. 5, pp.933–935.
- Polhamus, E.C. (1966) *A Concept of the Vortex Lift of Sharpedge Delta Wings based on a Leading-edge-suction Analogy*, Technical Report NASA TN D-3767, Langely Research Center, Langely Station, Hampton, Va.
- Rodríguez, I., Lehmkühl, O., Borrell, R. and Oliva, A. (2013) 'Direct numerical simulation of a NACA0012 in full stall', *International Journal of Heat and Fluid Flow*, 31 October, Vol. 43, pp.194–203.
- Slotnick, J., Khodadoust, A., Alonso, J., Darmofal, D., Gropp, W., Lurie, E. and Mavriplis, D. (2014) *CFD Vision 2030 Study: a Path to Revolutionary Computational Aerosciences*, May, NASA Technical Report, CR-2014-218178, NF1676L-18332.
- Spalart, P.R. and Allmaras, S.R. (1992) 'A one equation turbulence model for aerodynamic flows', *AIAA 30th Aerospace Sciences Meeting*, Reno, January.
- Taha, H.E., Hajj, M.R. and Beran, P.S. (2014) 'State-space representation of the unsteady aerodynamics of flapping flight', *Aerospace Science and Technology*, Vol. 34, pp.1–11.
- Tang, D. and Dowell, E.H. (2014) 'Experimental aerodynamic response for an oscillating airfoil in buffeting flow', *AIAA Journal*, Vol. 52, No. 6, pp.1170–1179.
- Taulbee, D.B. (1992) 'An improved algebraic Reynolds stress model and corresponding nonlinear stress model', *Physics of Fluids a: Fluid Dynamics (1989–1993)*, Vol. 4, No. 11, pp.2555–2561.
- Wang, Z.J., Birch, J.M. and Dickinson, M.H. (2004) 'Unsteady forces and flows in low Reynolds number hovering flight: two-dimensional computations vs. robotic wing experiments', *Journal of Experimental Biology*, Vol. 207, No. 3, pp.449–460.
- Wells, J.B., Salem-Said, A. and Ragab, S.A. (2009) *Effects of Turbulence Modeling on RANS Simulations of Tip Vortices*, PhD thesis, University Libraries, Virginia Polytechnic Institute and State University.
- Yarusevych, S. and Boutilier, M.S.H. (2011) 'Vortex shedding of an airfoil at low-Reynolds-numbers', *AIAA Journal*, Vol. 49, No. 10, pp.2221–2227.
- Yarusevych, S., Sullivan, P.E. and Kawall, J.G. (2009) 'On vortex shedding from an airfoil in low-Reynolds-number flows', *Journal of Fluid Mechanics*, Vol. 632, pp.245–271.

- Zakaria, M.Y., Al-Haik, M.Y. and Hajj, M.R. (2015a) 'Experimental analysis of energy harvesting from self induced flutter of a composite beam', *Applied Physics Letters*, Vol. 107, No. 2, p.023901.
- Zakaria, M.Y., Taha, H.E., Hajj, M.R. and Hussein, A.A. (2015b) 'Experimental-based unified unsteady nonlinear aerodynamic modeling for two-dimensional airfoils', in *33rd AIAA Applied Aerodynamics Conference*, p.3167.
- Zakaria, M.Y., Jafari, F. and Hajj, M.R. (2016) *Flow Measurements Associated with Lift Enhancement of a Plunging Airfoil Oscillating at High Angles of Attack and Reduced Frequencies*.
- Zakaria, M.Y., Taha, H.E. and Hajj, M.R. (2014) 'Shape and kinematic design optimization of the pterosaur replica', in *Proceedings of the 14th AIAA Aviation Technology, Integration, and Operations Conference*, Atlanta, GA, USA, pp.16–20.
- Zakaria, M.Y., Taha, H.E. and Hajj, M.R. (2017) 'Measurement and modeling of lift enhancement on plunging airfoils: a frequency response approach', *Journal of Fluids and Structures*, Vol. 69, pp.187–208.
- Zhou, Y., Alam, M.M., Yang, H., Guo, H. and Wood, D. (2011) 'Fluid forces on a very low-Reynolds-number airfoil and their prediction', *International Journal of Heat and Fluid Flow*, Vol. 32, No. 1, pp.329–339.